Polarized neutron reflectometry study of the magnetization reversal process in $YBa_2Cu_3O_7/La_{2/3}Ca_{1/3}MnO_3$ superlattices grown on $SrTiO_3$ substrates

J. Hoppler,[1,2] H. Fritzsche,[3] V. K. Malik,[1] J. Stahn,[2] G. Cristiani,[4] H.-U. Habermeier,[4] M. Rössle,[1] J. Honolka,[4] A. Enders,[4] and C. Bernhard[1,*]

[1]*Department of Physics and Fribourg Center for Nanomaterials, University of Fribourg, Chemin du Musée 3, CH-1700 Fribourg, Switzerland*

[2]*Laboratory for Neutron Scattering, Paul Scherrer Institut, CH-5232 Villigen PSI, Switzerland*

[3]*National Research Council Canada, Canadian Neutron Beam Centre, Chalk River Laboratories, Chalk River, Ontario, Canada K0J 1J0*

[4]*Max-Plank-Institut für Festkörperforschung Stuttgart, D-70569 Stuttgart, Germany*

(Received 23 November 2009; revised manuscript received 7 September 2010; published 29 November 2010)

Using polarized neutron reflectometry we investigated the reversal of the magnetization of a high-T_c superconductor/ferromagnet superlattice that consists of eight bilayers of $YBa_2Cu_3O_7$(25.6 nm)/$La_{2/3}Ca_{1/3}MnO_3$(25.6 nm) grown on a $SrTiO_3$ substrate. The measurements were performed during a magnetization hysteresis loop at 5 K. We obtained evidence that the reversal in the vicinity of the coercive field proceeds via the switching of micrometer-sized magnetic domains that are considerably larger than the typical domains of $La_{2/3}Ca_{1/3}MnO_3$. Furthermore, these large magnetic domains appear to be more strongly correlated along the vertical direction of the superlattice than along the lateral one. We provide evidence that this unusual behavior may be induced by the $SrTiO_3$ substrate which undergoes a series of structural phase transitions, some of which give rise to the formation of micrometer-sized surface facets that are tilted with respect to each other. These facets and the resulting strain fields are transmitted throughout the superlattice and thus may act as templates for the large magnetic domains in the $La_{2/3}Ca_{1/3}MnO_3$ layers whose magnetic properties are very susceptible to the lattice strain.

DOI: 10.1103/PhysRevB.82.174439 PACS number(s): 75.70.Cn, 75.70.Kw, 74.81.−g, 74.72.−h

I. INTRODUCTION

The similar in-plane lattice parameters of the oxides with perovskitelike crystal structure and the recent progresses in the sample growth techniques, have made it possible to grow artificial oxide heterostructures with well-controlled chemical and structural properties and, in particular, with atomically abrupt interfaces.[1,2] This development has stimulated great interest in the physical properties of these oxide heterostructures and has motivated many attempts to create artificial materials with new electronic interface states and with complex orders. The possibilities are manyfold since the individual materials offer a very wide spectrum of physical properties, ranging from ferroeletricity over ferromagnetism to high-temperature superconductivity.[3–5]

A recent example is the high mobility electron gas which develops between the insulating oxides $SrTiO_3$ (STO) and $LaAlO_3$ (Refs. 1, 2, and 6) whose carrier density can be largely varied by applying a gate voltage, thus allowing for a reproducible switching between insulating, metallic and even superconducting (SC) states.[6–8] Other prominent examples are heterostructures from materials with competing orders such as superconductivity and ferromagnetism. Studies on heterostructures from classical superconductors and s (FM) have already shown that the proximity coupling between these mutually exclusive orders can give rise to the formation of novel combined quantum states.[9] The corresponding quantum properties of the oxide-based counterparts, with the cuprate high-temperature superconductors and the ferromagnetic manganites that exhibit the so-called colossal magnetoresistance, may be even more fascinating and there is a fair chance that they can be realized at technologically relevant temperatures. Recent experiments on the oxide-based $YBa_2Cu_3O_7/La_{2/3}Ca_{1/3}MnO_3$ (YBCO/LCMO) multilayers have indeed revealed a number of remarkable phenomena such as (i) a strong suppression of the metalicity,[10] (ii) a giant magnetoresistance effect in LCMO/YBCO/LCMO trilayers which results from the dependence of the SC transition temperature on the relative orientation of the FM moments in the LCMO layers,[11] (iii) an unusually strong photodoping effect of the SC transition temperature,[12] (iv) a so-called antiphase proximity effect in high-T_c superconductor/ferromagnet heterostructures where a ferromagnetic moment is induced in the YBCO layer that is antiparallel with respect to the one in the neighboring LCMO layer,[13,14] and (v) the observation of a giant superconductivity-induced modulation of the ferromagnetic order in the LCMO layers.[15]

These experiments have established that the electromagnetic properties of these oxide heterostructures are extremely versatile and can be readily modified by various kinds of perturbations such as electric and magnetic fields and even by the onset of superconductivity in a neighboring layer.[15] At the same time they provided first clear indications that the electromagnetic properties of these heterostructures may be strongly dependent on external factors such as the strain that is transmitted from the substrate. The commonly used STO substrates are indeed well known to undergo a series of structural phase transitions as a function of temperature between 10 and 300 K. Furthermore, it was recently shown that these phase transition can be accompanied by the formation of structural domains and a subsequent faceting of the surface (with a buckling of up to 0.5°) of the STO substrates that is translated into the thin film grown on top.[16] The re-

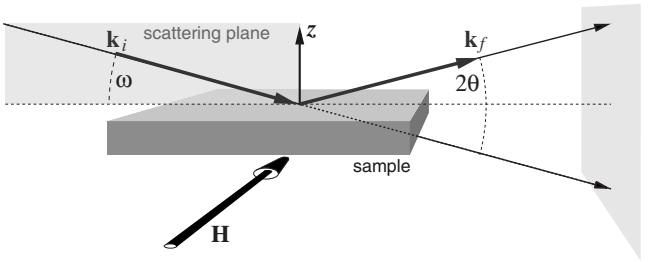

FIG. 1. Sketch of the geometry of the neutron beams and the applied magnetic field, **H**, for the neutron reflectometry measurements. The scattering plane is spanned by the incident beam $\mathbf{k}_i$ and the final beam $\mathbf{k}_f$ and contains the surface normal **z**. The angle of incidence relative to the (averaged) surface is denoted as ω while the scattering angle (detector angle) is 2θ. For the experiments presented here, **H** is applied normal to the scattering plane.

sulting strain fields have been shown to strongly influence the formation of the magnetic domains in LCMO layers[17] as well as in (YBCO/LCMO) multilayers.[15]

In this paper we further explore the complex behavior of the magnetic domains in thin film YBCO/LMCO multilayers with magnetic field dependent polarized neutron reflectometry (PNR) measurements. From these we obtain direct information about the magnetization reversal process and thus about the extent and the coupling of the magnetic domains in the lateral and the vertical directions of the superlattice. We find that the magnetic domains are micrometer sized and strongly coupled in the vertical direction and likely are controlled by the structural domains of the substrate and their strain fields which are transmitted into the multilayer.

II. POLARIZED NEUTRON REFLECTOMETRY

The technique of specular neutron reflectivity enables one to probe the depth profile of the nuclear and the magnetic potentials of thin films and heterostructures. As sketched in Figs. 1 and 2 the incoming neutron wave (with vector $\mathbf{k}_i$) is totally or partly reflected at a surface or at a series of parallel interfaces.[18] All (multiply) reflected waves interfere and thus the intensity of the wave leaving the surface (with vector $\mathbf{k}_f$) is affected by the individual potential contrasts at the interfaces, the distances between them and the momentum transfer normal to the surface $q_z = |\mathbf{k}_f - \mathbf{k}_i|$. Assuming a lateral uniform density in the sample and elastic scattering, no in-plane momentum transfer occurs. Figure 1 illustrates the geometry of a specular reflectivity setup. Reflectometry measurements do not resolve atomic dimensions but they probe a potential that is laterally averaged on the micrometer scale. Thus one introduces an average potential $V(z)$ and an index of refraction in analogy to optics

$$n(z) = \sqrt{1 - V(z)/E} := 1 - \delta(z) \tag{1}$$

$$\approx 1 - V(z)/2E, \quad \text{for } V(z)/E \ll 1 \tag{2}$$

with the free neutron energy $E = E^{\text{kin,vacuum}} = m_n v^2/2 = 2\pi^2\hbar^2/m_n\lambda^2$. The potential $V(z)$ contains nuclear contributions $V^{\text{nuc}} \propto \rho^b(z)$ (the laterally averaged neutron

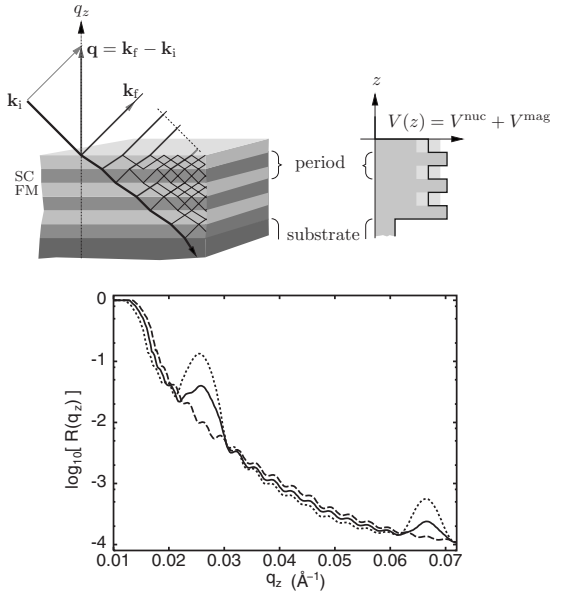

FIG. 2. Illustration of the wave fields formed in a multilayer by refraction and multiple reflection at the interfaces (top left); and the corresponding depth profile of the potential V (top right). The solid line in the depth profile stands for the nuclear contribution, the shaded areas mark the potential including magnetic contributions for $|-\rangle$ and $|+\rangle$ neutrons. The graph shows a calculated $R(q_z)$ curve for a nonmagnetic sample (solid line) and for the case where one material is magnetic. The dotted line corresponds to spin-down, the dashed one to spin-up neutrons.

scattering length density) and the magnetic scattering potential $V^{\text{mag}} = \boldsymbol{\mu}_n \mathbf{B}_\perp$ with the components of the magnetic induction **B** normal to the scattering vector **q** and the neutron magnetic moment $\boldsymbol{\mu}_n$. By substituting for (depth dependent) material properties and neutron wavelength λ for V and E, one obtains

$$\delta(z) = \underbrace{\frac{\lambda^2}{2\pi}\sum_i^{\rho^b(z)} \rho_i(z) b_i}_{\delta^{\text{nuc}}(z)} + \underbrace{\frac{\lambda^2}{2\pi} \cdot \frac{-m_n}{2\pi\hbar^2} \boldsymbol{\mu}_n \mathbf{B}_\perp(z)}_{\delta^{\text{mag}}(z)} \tag{3}$$

with the number density ρ_i and the nuclear scattering length b_i, where the index i runs over all isotopes. Both, δ^{nuc} and (if present) δ^{mag} are on the order of 10^{-7} to 10^{-6}, which justifies the step from Eq. (1) to Eq. (2). Since the sign of δ^{mag} depends on the neutron spin polarization relative to **B**, it is possible to extract $\mathbf{B}_\perp$ from difference in the reflectivities for both polarizations

$$B_\perp = \frac{2\pi\hbar^2}{m_n \mu_n} \cdot \frac{\delta^{\text{mag}}}{\lambda^2/2\pi}. \tag{4}$$

The index $\perp$ of $\mathbf{B}_\perp$ indicates, that only the components normal to the scattering vector **q** are relevant. This still leaves a degree of freedom for the direction of $\mathbf{B}_\perp$ relative to the magnetic moment $\boldsymbol{\mu}_n$ of the neutrons. $\boldsymbol{\mu}_n$ is either parallel (spin up, +) or antiparallel (spin down, −) to the externally applied magnetic field **H**. In most cases (including the present one) **H** is chosen to be normal to the scattering plane

(see Fig. 1). The component of $\mathbf{B}_\perp$ parallel to $\boldsymbol{\mu}_n$ leads to scattering which preserves the neutron spin state while the perpendicular component (also in the sample plane) causes a flip of the spin (not studied here).

In analogy to the nuclear term in Eq. (3) one can define $\delta^{\text{mag}} := \lambda^2/2\pi \cdot \Sigma_j \rho_j p_j$ with the magnetic scattering lengths p_j. The index j runs over all nonsymmetry equivalent atoms (in contrast to i in b_i, which disregards symmetry, but differentiates the isotopes). If one assumes that the magnetic moments can be assigned to a single lattice site j, the following Ansatz is possible:

$$\mathbf{B} = \mu_0 \rho_j \boldsymbol{\mu}_j, \tag{5}$$

which together with Eq. (4) allows to evaluate the magnetic moment $\boldsymbol{\mu}_j$ from δ^{mag} which is obtained from the measurements. Figure 2 shows a sketch of the sample (a heterostructure consisting of equally thick layers of superconductors, SC, and ferromagnet, FM, a related profile of the potential $V(z)$, and simulated reflectivity curves. Since for most materials δ is positive for neutrons, one gets total external reflection at low q_z, i.e., $R(q_z)=1$ for $q_z < q^c$. The critical momentum transfer q^c describes the situation, where the refracted beam travels along the surface. Using Snell's law this means $q_c = 4\sqrt{\pi\rho} \propto \sqrt{V}$. Thus q_c measures the mean density of the sample close to the surface. In Fig. 2 this can be seen by the shift of q_c for spin-up $(\rho^{\text{nuc}} + \rho^{\text{mag}})$ and spin-down neutrons $(\rho^{\text{nuc}} - \rho^{\text{mag}})$.

Above q_c the reflectivity decreases rapidly and approaches the asymptote $(4q_z/q_c)^{-4}$. If the sample consists of a periodic structure one gets constructive interference like in a one-dimensional crystal. The resulting peaks in $R(q_z)$ are therefore often called Bragg peaks (the strong refraction effect for samll ω demands for applying Bragg's law in the dynamical limit, here). From the distances of these Bragg peaks one can derive the period length, their intensities tell the contrast at the interfaces and the thickness ratios within a period. In special cases one can even get the extinction of peaks as, for example, for a layer thickness ratio of 1:1. There all even order peaks are forbidden by symmetry. Figure 2 shows this absence of the second-order Bragg peaks at $q_z \approx 0.045$ Å^{-1}. At the same time the contrast $V_{\text{SC}}/V_{\text{FM}}$ is strongly affected by the magnetization: for spin-up neutrons it almost vanishes (i.e., $V_{\text{SC}} \approx V_{\text{FM,up}}$), while for spin-down it is increased. The surface and the interface to the substrate limit the periodic structure and introduce additional interference terms which lead to the rapid oscillations (Kiessig fringes) on $R(q_z)$.

Since $R(q_z)$ does not contain the information about the phase of the interferences, there is no direct way to determine $V(z)$ from the measurement. Instead one has to build a model, calculate $V(z)$ and $\delta(z)$ and then one has to use some idealized method to calculate $R(q_z)$. The model has to be refined and adjusted until the measurements (or at least some interesting features) are adequately reproduced. For the derivation of the reflectance and reflectivity from $V(z)$ please refer to Refs. 18 and 19.

For typical neutron wavelengths of fractions of a nanometer the angle of incidence is on the order of a degree (gracing incidence). Due to their relatively weak interaction with most materials, the probe depth of neutrons is on the order of a micrometer (μm). Accordingly, neutron reflectometry usually probes all the layers and interfaces of thin-film-based heterostructures.

The region over which this method averages in the lateral direction is on the μm scale. Lateral inhomogeneities on this or a shorter scale lead to a faster decay of $R(q_z)$ and the Bragg peak intensities due to scattering processes in nonspecular directions. Inhomogeneities on a larger scale lead to a superposition of the reflectivities of the individual regions (domains).

The reflectometers used for the presented studies, C5 at Chalk River, Canada, and ADAM at ILL, France, are operating in the angle-dispersive mode. This means the reflectivity is measured as a function of the angle of incidence ω while keeping the wavelength λ fixed. The incoming neutron beam is defined by slits and eventually polarized. The sample is rocked relative to the incident beam and the detector rotates around the sample at an angle 2ω.

III. SAMPLE CHARACTERIZATION AND EXPERIMENTAL SETUPS

The investigated superlattice have the composition $[\text{LCMO}(25.6\ \text{nm})/\text{YBCO}(25.6\ \text{nm})]_8/\text{STO}_{(001)}$, i.e., it consists of eight bilaleyers of $La_{2/3}Ca_{1/3}MnO_3$ and $YBa_2Cu_3O_7$, grown by pulsed laser deposition on the (001) oriented surface of an as polished and cleaned 1×1 cm^2 $SrTiO_3$ substrate as described in Refs. 10 and 20. The thickness of the individual layers of 25.6 nm has been confirmed by unpolarized neutron reflectometry measurements at 300 K. The macroscopic superconducting and magnetic properties have been determined with dc magnetometry measurements on a small piece that has been cut from the corner of the sample. They yield a ferromagnetic transition temperature $T_{\text{Curie}}=240$ K, a superconducting transition temperature $T_{\text{sc}}=82$ K, a coercive field $\mu_0 H_{\text{coerc}}=0.028$ T and a saturation moment of 2.9 μ_B per Mn at $\mu_0 H_{\text{appl}}=7$ T and 5 K (see Fig. 3).

The specular PNR measurements have been performed at the instrument C5 at the Chalk River Laboratories in Canada. The sample was inserted in a cryomagnet (Oxford instruments) where it was cooled to 5 K in zero magnetic field and then saturated in $\mu_0 H_{\text{appl}}=7$ T before measuring on the M-H-hysteresis loop from −7 to +7 T. The exact value of the magnetic field has been subsequently measured with a Hall probe sensor that was placed in the sample position of the cryomagnet. It was found to be within 4% of the nominal field with an offset of 0.0021 T due to some remanence in the cryomagnet after saturation at ±7 T.

The PNR measurements have been performed during a M-H-hysteresis loop of up to 7 T. The reflection curves were measured in the saturated state at a very high field of 6 T and at representative low fields which track the magnetization reversal process around the coercive field of $\mu_0 H_{\text{coerc}}=0.028$ T. For high magnetic fields (>0.1 T) the guide field that is required to maintain the neutron spin polarization was provided by the stray field of the sample magnet. This stray field changes its direction along the flight path of the neutrons such that the magnetic field at the sample is

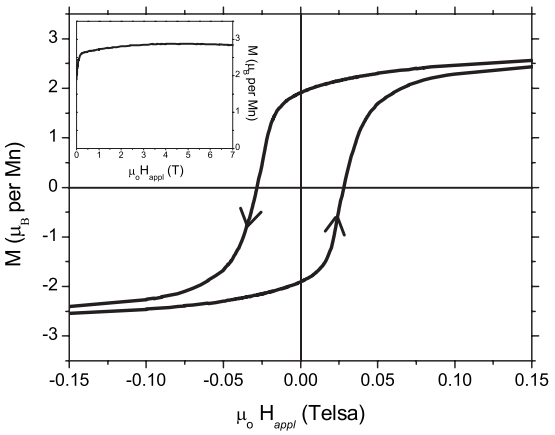

FIG. 3. Magnetization loop of the $[YBa_2Cu_3O_7(25.6\ nm)/La_{2/3}Ca_{1/3}MnO_3(25.6\ nm)]\times 8$ superlattice performed with a vibrating sample magnetometer at $T=5$ K. The main part shows the low field regime which yields a coercive field of $\mu_0 H_{coerc}=0.028$ T and the absence of an exchange bias effect. The inset displays the positive branch up to 7 T from which a saturation moment of about 2.9 μ_B per Mn is derived. The diamagnetic signal of the $SrTiO_3$ substrate has been subtracted.

antiparallel to the one at the polarizer. To ensure that the neutrons can adiabatically follow the guide field, the sample magnet needs to be operated in an asymmetric mode where the low-field regime is not accessible.[21,22] For the low fields (<0.1 T) we thus used an additional guide field device that is installed between the polarizer and sample magnet and maintains the same magnetic field direction between the polarisers and the sample. Accordingly, the *high-field* measurements have been performed at $\mu_0 H<-0.1$ T, and the *low-field* measurements in the range $0<\mu_0 H<+0.1$ T. For the following discussion we assumed that the hysteresis loop is symmetric to the origin. This assumption is supported by the *M*-*H*-hysteresis loop as measured with a dc magnetometer and shown in Fig. 3.

In addition, we performed off-specular PNR measurements at the Institute Laue Langevin (ILL) in Grenoble, France using the polarized angle-dispersive reflectometer ADAM.

IV. EXPERIMENTAL RESULTS

Figure 4 documents the evolution of the specular PNR curves at $T=5$ K during the magnetization reversal process. It shows representative reflectivity curves in remanence (a), during the reversal (b) and (c), right after the reversal (d), and in saturation (e). We begin with the discussion of the PNR curves in the remanent state in Fig. 4(a) that was achieved by magnetising the sample in a magnetic field of $\mu_0 H_{appl}=7$ T and reducing the field to $\mu_0 H_{appl}=0.008$ T. For comparison we also show an unpolarized reflectivity curve in the non magnetic state that was obtained at room temperature. The PNR curves exhibit a clear splitting between the spin-up and spin-down states ($|+\rangle, |-\rangle$) of the neutrons at the edge of total reflection as well as at the first Bragg peak of the superlattice. In both cases, the intensity is

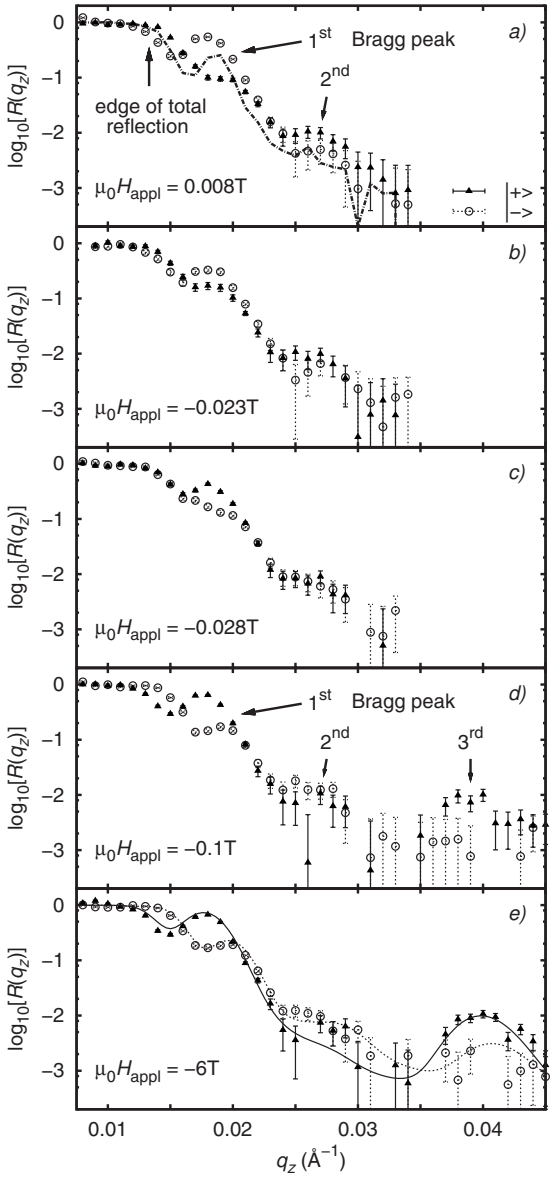

FIG. 4. PNR curves taken at 5 K right before (a), during [(b) and (c)] and after the magnetization reversal process (d) and finally in saturation (e). The up (down) triangles show the curves for the spin-up (spin-down) polarization of the neutron spins, i.e., for $|+\rangle$ ($|-\rangle$). The dashed line in (a) shows the unpolarized reflectivity curve at room temperature in the nonmagnetic state, the solid lines in (e) show reflectivity curves that were calculated with a model as described in the text.

enhanced for the $|-\rangle$ state (as compared to the unpolarized spectrum) and reduced for the $|+\rangle$ state. These splittings indicate that the sample has a sizable net magnetization in the direction parallel to the applied magnetic field. While the splitting of the reflection edge is dominated by the magnetization of the topmost LCMO layers of the superlattice, the one of the first Bragg peak is proportional to the average magnetization of all LCMO layers. We note that the YBCO layers are nominally nonmagnetic, even though it was previously shown that small proximity-induced Cu moments can develop in the YBCO layers Refs. 13 and 14. For superlattices with equally thick YBCO and LCMO layers, these give

rise to a slight enhancement of the intensity at the structurally forbidden second Bragg peak Refs. 13 and 14. A corresponding weak effect on the second Bragg peak also occurs for the present superlattice. Nevertheless, since we are mainly concerned with the reversal behavior of the much larger moments in the LCMO layers, the details of the second-order Bragg peak are not further discussed here.

Upon further reduction and reversal of the applied field, the splitting between the curves of the two neutron spin states becomes considerably reduced in magnitude at −0.023 T [Fig. 4(c)], before it almost vanishes and changes its sign around the coercive field of −0.028 T [Fig. 4(c)] as determined from the dc magnetometry measurement (see Fig. 3). Finally, the splitting increases again and reaches its full magnitude (with an inverted sign) at −0.1 T and −6 T [Figs. 4(d) and 4(e)]. This observation that the sign reversal of the splitting of the reflection edge and the first Bragg peak of the PNR curves both occur in the vicinity of $\mu_0 H_{\mathrm{coerc}} = -0.028$ T, suggests that all LCMO layers, including the ones at the top and the bottom of the superlattice, are undergoing a similar and synchronous magnetization reversal process.

For a quantitative analysis of the shape and the magnitude of the vertical profile of the magnetization density we performed model calculations and compared them with the experimental PNR curves. In a first attempt, we used a code written by Kentzinger that is based on the Parrat formalism.[23] This formalism assumes a certain depth profile of the magnetization density in the vertical direction of the superlattice and a homogeneous magnetization in the lateral direction. If the magnetization is not homogeneous but consists of domains much smaller than the coherence volume, the specular reflectivity is given by the lateral average of the magnetization. In this case the inhomogeneities lead to off-specular scattering and thus a reduction in the specular intensity. This can approximately be taken into account by an increased "magnetic roughness" when calculating $R(q_z)$. More accurate, and indispensable in the case where the domain sizes are on the order of the neutron coherence length, is the treatment within the distorted wave born approximation.[24]

As shown by the solid and dotted lines in Fig. 4(e), this model yields a reasonable description of the PNR curves in the saturated state at −6 T. For this we used a vertical profile of the magnetization density that is similar to the one presented in Ref. 13. The magnitude of the magnetic moments in the LCMO layers varies between 3.0 and 3.5 μ_B per Mn ion depending on how the magnetic moment is assumed to evolve around the YBCO/LCMO interfaces. Its magnitude thus agrees fairly well with the value of 2.9 μ_B per Mn as obtained from the saturation value of the dc magnetization data (see Fig. 3).

To the contrary, with this model we failed to obtain a reasonable description of the PNR curves at low fields in the vicinity of the coercive field. This is demonstrated in Fig. 5 which shows that the PNR curves for the $|+\rangle$ and the $|-\rangle$ states of the neutrons at −0.023 T cannot be reproduced with the same depth profile of the magnetization density. The best fit to the $|-\rangle$ curve as shown in Fig. 5(a) severely underestimates the strength of first-order Bragg peak of the $|+\rangle$ curve

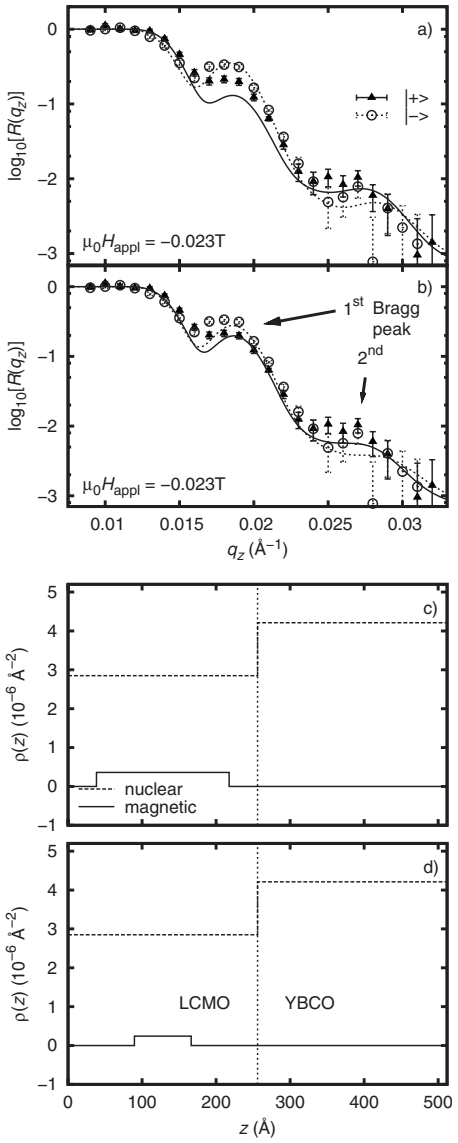

FIG. 5. (a) and (b) Comparison of the measured polarized reflectivity curves at $\mu_0 H_{\mathrm{appl}} = -0.023$ T close to the coercive field (points with error bars) with representative fits using a model that assumes a coherent superposition of the signal from small magnetic domains (as compared to the neutron coherence volume). It shows that a good fit to the spin-down channel results in a very poor fit for the spin-up channel (a) and vice versa (a). (c) and (d) Magnetic depth profiles that have been used for the fits in (a) and (b), respectively.

(note the logarithmic scale). Equally well, as shown in Fig. 5(b), we find that a model which reproduces the $|+\rangle$ curve, provides only a poor description of the much stronger first-order Bragg peak in the $|-\rangle$ signal. Figures 5(c) and 5(d) show the depth profile of the magnetic and nuclear potential based on which the fits in Figs. 5(a) and 5(b) have been obtained. This failure to reproduce the experimental data suggests that some of the assumptions underlying our theoretical model are not met by our sample. As outlined below, the most likely explanation is that the magnetic domains are significantly larger than the coherence length of the neutron beam. Other possibilities, like an in-plane or an out-of-plane

rotation of the magnetization or a layer by layer switching of the magnetization density of the individual LCMO layers can be ruled out. The latter would modify the depth profile of the magnetization density and thus would give rise to structures in $R(q_z)$ in addition to the edge of total reflection and the regular Bragg peaks. The out-of-plane rotation is unlikely since the out-of-plane axis is a hard axis as shown by the dc magnetization measurements (not shown here). Concerning the in-plane rotation, it has been demonstrated by Radu *et al.*,[25] that it introduces an additional steplike structure at the reflection edge. Upon the rotation of the homogeneous magnetization the splitting between the edges for the $|+\rangle$ and $|-\rangle$ channels would remain unchanged while the intensities of these edges would vary and finally become exchanged. Figure 4 illustrates that such a behavior, i.e., a change in intensity rather than a change in the q_z position of the $|+\rangle$ and $|-\rangle$ reflection edges, is not observed during the magnetization reversal of our sample.

According to the above considerations, our next attempt is to model the magnetization reversal process in terms of a flipping of very large magnetic domains whose lateral size exceeds the coherence length of the neutron beam of about 10 μm. In that case, the total neutron signal consists of an incoherent superposition of the contributions of these large domains. The absence of additional structures in our PNR curves (besides the reflection edge and the regular Bragg peaks) requires again that the flipping of the magnetization in these domains is strongly correlated in the vertical direction, or in other words, that the shape of the vertical profile of the magnetization density within the individual domains is maintained during the reversal process. The PNR signal thus should consist of an incoherent superposition of the reflectivity signals from domains that are either in the remanent or in the reversed state. Accordingly, it should be possible to describe the data by using a linear combination of the PNR curves that have been measured in the saturated state at large positive and negative fields, respectively.

Figure 6 shows that this approach provides indeed a fairly good description of our experimental data. It confirms that all our experimental curves in the range of $\mu_0 H_{\mathrm{appl}}$=0.008 T to −0.048 T around the coercive field can be reasonably well reproduced with a linear combination of the experimental PNR curves at $\mu_0 H_{\mathrm{appl}}$=0.008 T and −0.048 T according to the equation

$$R^{\pm} = xR^{\pm}_{-0.048\ \mathrm{T}} + (1-x)R^{\pm}_{0.008\ \mathrm{T}}. \tag{6}$$

The relevancy of this model has been checked by performing the same kind of analysis to the M-H-hysteresis loop in the macroscopic dc magnetization data. The evolution of the total magnetization is described here in terms of a linear combination of the values measured in remanence at $\mu_0 H_{\mathrm{appl}}$=0.008 T and at $\mu_0 H_{\mathrm{appl}}$=−0.048, according to the equation

$$M = xM_{-0.048\ \mathrm{T}} + (1-x)M_{0.008\ \mathrm{T}}. \tag{7}$$

The x values as obtained from the analysis of the PNR and dc magnetometry data are listed in Table I which shows that the general trends agree rather well. The small differences in the absolute values may suggest that the vertical

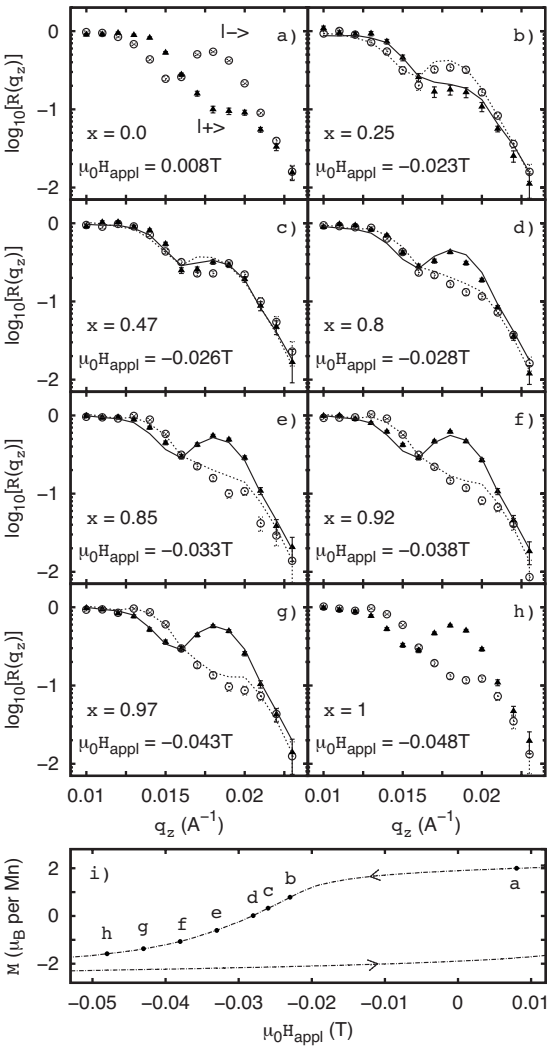

FIG. 6. (a)–(h) Measured reflectivity curves during the reversal process (points with error bars). The data during magnetization reversal are shown to be reasonably described by a linear combination of the reflectivity curves measured at $\mu_0 H_{\mathrm{appl}}$=0.008 T and $\mu_0 H_{\mathrm{appl}}$=−0.048 T. The lines in the figures are calculated with the formula $R^{\pm}=xR^{\pm}_{-0.048\ \mathrm{T}}+(1-x)R^{\pm}_{0.008\ \mathrm{T}}$ with x given in the respective figure. (i) Measured M-H-hysteresis loop with the points indicated where the reflectivity curves (a)–(h) have been measured.

coupling is not fully maintained, at least not in all of these zones. This could also explain the minor deviations of the data from the linear combinations as shown in Fig. 6.

Irrespective of these deviations, our result suggests that the magnetization switching in these superlattices involves some surprisingly large domains that are strongly coupled in the vertical direction, i.e., across the 25.6-nm-thick $YBa_2Cu_3O_7$ layers. In comparison, the lateral coupling between these micrometer-sized zones appears to be significantly weaker.

Such a behavior may be explained in terms of the structural surface facets which previously have been shown to develop below a structural transition of the $SrTiO_3$ substrate at $T_{\mathrm{STO}} \approx 65$ K.[16] These facets are tilted with respect to each other and divide the sample into separate zones which extend over tens of micrometer in the lateral directions and are

TABLE I. x values of the linear combination $M(\mu_0 H_{\text{appl}}) = xM_{-0.048\ \text{T}} + (1-x)M_{0.008\ \text{T}}$ as determined from magnetometry measurements compared with x values determined from PNR measurements by $R^{\pm} = xR^{\pm}_{-0.048\ \text{T}} + (1-x)R^{\pm}_{0.008\ \text{T}}$.

$\mu_0 H_{\text{appl}}$	$x_{\text{magnetometry}}$	$x_{\text{reflectometry}}$
0.008 T	0.0	0.0
−0.023 T	0.34	0.25
−0.026 T	0.47	0.47
−0.028 T	0.56	0.8
−0.033 T	0.73	0.85
−0.038 T	086	0.92
−0.043 T	0.94	0.97
−0.048 T	1.0	1.0

transmitted through the entire superlattice.[16] Accordingly, the borders of the facets and the resulting strain fields are penetrating the entire superlattice. Since the magnetic properties of $La_{2/3}Ca_{1/3}MnO_3$ are well known to be strongly dependent on the lattice strain, it is possible that these borders exhibit a much softer magnetic (or even nonmagnetic) behavior than the core regions of the facets. The coupling within the latter is likely dominated by the intrinsic domains of $La_{2/3}Ca_{1/3}MnO_3$ which are typically much smaller, i.e., in the order of several hundred nanometers,[26,27] and therefore not resolved in our PNR experiment. All we can tell from our measurements is that within each of the individual micrometer-sized domains the switching of the nanodomains seems to occur in a collective manner at a well defined field. Between the facets, these switching fields apparently exhibit some significant variation.

Direct evidence for the existence of such micrometer-sized domains has been obtained from off-specular neutron reflectometry measurements with spin-down neutrons on the same sample. Figure 7 shows so-called reflectivity maps at temperature of 300 K (a) and 15 K (b) where the intensity of the neutron reflectivity signal is plotted as a function of the angle of the incident beam α_i versus the angle of the scattered beam α_f. The gray scale shows the logarithm of the measured neutron intensity. The specular reflectivity requires that $\alpha_i = \alpha_f$ and thus occurs along the diagonal through the

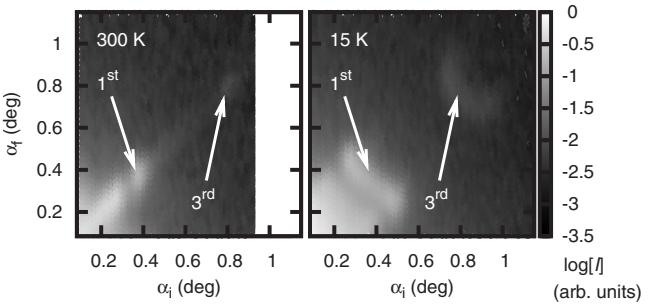

FIG. 7. Off-specular maps at temperature of 300 K (a) and 15 K (b) plotted as a function of the angle of the incident beam, α_i, versus the one of the reflected beam, α_f. The significant broadning of the specular signal in (b) arises from the buckling of the sample surface which gives rise to an angular spread of about 0.3°–0.4°.

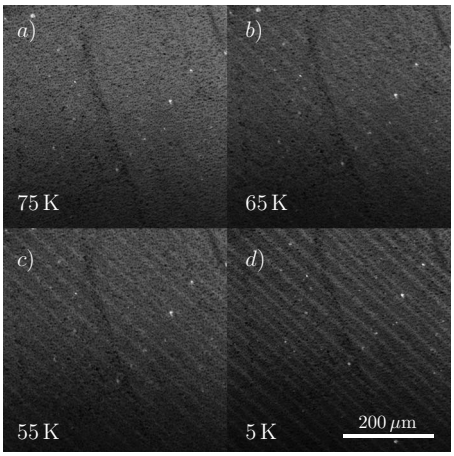

FIG. 8. Magneto-optical images showing the occurrence of a domain state on the micrometer scale which appears as a stripelike variation from bright to dark contrast along the diagonal direction of the sample. This domain state is most pronounced at 5 K and disappears above 65 K.

origin of these maps. For the spectrum at 300 K it is evident that the major part of the neutron signal is confined to this specular range. The some of the characteristic feature like the first- and third-order Bragg peaks are marked by arrows. To the contrary, in the 15 K spectrum the neutron signal is spread out over a much wider region in the off-specular direction. More specifically, the reflection edge and the Bragg peaks are broadened in the direction perpendicular to the specular line. It appears that the signal consists of a superposition of several quasispecular reflectivity curves whose crossing points with the α_i axis are shifted away from the zero position. This behavior is characteristic of a buckling of the sample surface which yields large facets (on the order of the coherence length of the neutron beam of about 10 μm) that are tilted with respect to each other by angles as large as 0.3°–0.4° [as can be directly seen from Fig. 7(b)]. This behavior has already been identified and discussed in Refs. 15 and 16, where it was shown that the buckling arises due to a structural transition of the STO substrate around 65 K, likely driven by the strain fields that arise at the boundaries of differently oriented domains. This buckling and likely also the associated strain fields get translated into the multilayer that is grown on top.

A real-space image of these large scale domains has been obtained from magneto-optical imaging experiments on the same sample as shown in Fig. 8. The image at 5 K in Fig. 8(d) reveals a pronounced and regular pattern of strongly anisotropic magnetic domains that extend along the diagonal direction of the film plane. The typical size of these domains is on the scale of several tens of micrometers along one direction and even many hundreds of micrometers along the other one. Accordingly, it is most likely the flipping of these domains that determines our PNR curves. A detailed report on the temperature and magnetic field dependence of these magneto-optical images will be represented in a forthcoming publication.[28] Here we only remark that the formation of these large magnetic domains is indeed linked with the structural phase transitions of the $SrTiO_3$ substrate as can be seen

from the image at 75 K in Fig. 8(a), where the domain pattern is absent. In addition, We notice that a similar behavior was previously observed in individual $La_{2/3}Ca_{1/3}MnO_3$ films grown on $SrTiO_3$.[17]

V. DISCUSSION

Our observations have implications not only for the understanding of the physical properties of the oxide-based multilayers from cuprate high-temperature superconductors and ferromagnetic manganites but also for the general field of heterostructures from complex oxides. In the first place, they manifest that the electromagnetic properties of these oxide-based heterostructures can be extremely versatile and thus strongly affected and modified by various kinds of intrinsic and extrinsic parameters. In the present case, our specular PNR measurements have shown that the magnetization reversal in the $[YBa_2Cu_3O_7(25.6\ nm)/La_{2/3}Ca_{1/3}MnO_3(25.6\ nm)]\times 8$ superlattice proceeds via the flipping of magnetic domains that are surprisingly large (in excess of 10 μm) and strongly correlated along the vertical direction. Our additional off-specular reflectometry measurements suggest that this unusual behavior is caused (or at least strongly influenced) by the buckling of the surface region of the STO substrate that occurs below a structural phase transition of about 65 K. This buckling gives rise to the formation of very large surface facets that are tilted with respect to each other by up to 0.4°. This buckling is transmitted into the superlattice and the large strain fields at the borders of the tilted facets likely give rise to a strong modification of the magnetic properties of the $La_{2/3}Ca_{1/3}MnO_3$ layers. We suspect that the highly strained regions at the borders between the facets exhibit a much softer ferromagnetic (or even a nonferromagnetic) behavior than the ones near the cores of the facets. Such a strain-induced template of the magnetic properties would explain that the switching fields of these micrometer-sized magnetic domains are almost identical along the vertical direction while they vary considerably along the lateral one.

It is interesting that a very different reversal mechanism has been reported for similar heterostructures that were grown by high-pressure dc sputtering.[11,29] In samples with a YBCO layer thickness of less than 35 nm the *M*-*H*-hysteresis loop revealed a steplike behavior which is indicative of a layer-by-layer magnetization reversal. We can only speculate that this clear difference with respect to the behavior in our sample is related to the different growth process and a resulting difference in the nature and the strength of the coupling between the individual layers. Another difference concerns the fact that in their samples the first LCMO layer was directly grown on the STO substrates. This may give rise to a strongly modified magnetic behavior of this first LMCO layer. In our sample, we first grew a YBCO layer which acts as a buffer between LCMO and the $SrTiO_3$ substrate and ensures that the LCMO layers experience similar strain conditions. It is also possible that the formation of the structural facets strongly depends on the quality of the $SrTiO_3$ substrates and thus may exhibit a large variation between different seemingly identical samples.

At present we can only speculate whether this strain-induced phenomenon may be useful for applications. For example, with the use of templated substrates it may enable one to determine the size, shape, and geometry of the magnetic domains of the LCMO layers. The variation in the local strain may also be used to design regions with larger and smaller coercive fields and with a larger or weaker coupling along the vertical direction. There may also exists other kinds of oxide-based heterostructures whose physical properties can be strongly modified with the strain that is transmitted from a patterned substrate. Certainly, this will require different kinds of substrate materials or higher-quality single-crystalline STO substrates whose surfaces can be patterned under well-controlled conditions.

VI. SUMMARY

In summary, with PNR measurements we observed a rather unusual magnetization reversal process in a $[25.6\ nm/25.6\ nm]\times 8$ superlattice of $YBa_2Cu_3O_7/La_{2/3}Ca_{1/3}MnO_3$ that has been grown by pulsed laser deposition on a (001) oriented $SrTiO_3$ substrate. We found that the magnetization reversal behavior during a so-called magnetization loop is determined by the switching of very large ferromagnetic domains with a lateral extent of at least tens of micrometers. In the vertical direction these switching fields appear to be strongly correlated while in the lateral direction they exhibit a rather broad and continuous variation. This result is remarkable, since magnetic domains in LCMO are typically much smaller, i.e., on the order of hundreds of nanometers,[26,27] and their coupling across a 25.6-nm-thick $YBa_2Cu_3O_7$ layer is expected to be fairly weak. We interpret our data in terms of a strain induced modification (templating) of the magnetic properties of the LCMO layers that arises from a buckling of the surface region of the $SrTiO_3$ substrate which occurs below a structural transition at $T_{STO}\approx 65$ K (Ref. 16) 65 K. Our off-specular neutron reflectometry measurements confirm that the resulting pattern of micrometer-sized, tilted facets is transmitted into the superlattice that is grown on top. Our conjecture is furthermore supported by the direct observation of a similar pattern of micrometer-sized magnetic domains by means of magneto-optical imaging experiments.

ACKNOWLEDGMENTS

The PNR experiments presented in this work have been performed at C5 at the Chalk River Laboratories, Canada, and at Adam at the ILL in Grenoble, France. For his assistance with the latter we thank M. Wolff. This work has been supported by the Swiss National Foundation under Grants No. 200020-119784 and No. 200020-129484 as well as by the NCCR program MaNEP.

*christian.bernhard@unifr.ch

[1] A. Ohtomo, D. A. Muller, J. L. Grazul, and H. Y. Hwang, Nature (London) **419**, 378 (2002).
[2] A. Ohtomo and H. Y. Hwang, Nature (London) **427**, 423 (2004).
[3] H. J. Bakker, S. Hunsche, and H. Kurz, Rev. Mod. Phys. **70**, 523 (1998).
[4] M. B. Salamon and M. Jaime, Rev. Mod. Phys. **73**, 583 (2001).
[5] R. J. Cava, B. Batlogg, R. B. van Dover, D. W. Murphy, S. Sunshine, T. Siegrist, J. P. Remeika, E. A. Rietman, S. Zahurak, and G. P. Espinosa, Phys. Rev. Lett. **58**, 1676 (1987).
[6] S. Thiel, G. Hammerl, A. Schmehl, C. W. Schneider, and J. Mannhart, Science **313**, 1942 (2006).
[7] A. D. Caviglia, S. Gariglio, N. Reyren, D. Jaccard, T. Schneider, M. Gabay, S. Thiel, G. Hammerl, J. Mannhart, and J.-M. Triscone, Nature (London) **456**, 624 (2008).
[8] C. Cen, S. Thiel, J. Mannhart, and J. Levy, Science **323**, 1026 (2009).
[9] L. Bulaevskii, A. Buzdin, and M. Maley, Phys. Rev. Lett. **90**, 067003 (2003).
[10] T. Holden, H. U. Habermeier, G. Cristiani, A. Golnik, A. Boris, A. Pimenov, J. Humlicek, O. I. Lebedev, G. Van Tendeloo, B. Keimer, and C. Bernhard, Phys. Rev. B **69**, 064505 (2004).
[11] V. Peña, Z. Sefrioui, D. Arias, C. León, J. Santamaria, J. L. Martinez, S. G. E. te Velthuis, and A. Hoffmann, Phys. Rev. Lett. **94**, 057002 (2005).
[12] V. Peña, T. Gredig, J. Santamaria, and I. K. Schuller, Phys. Rev. Lett. **97**, 177005 (2006).
[13] J. Stahn, J. Chakhalian, Ch. Niedermayer, J. Hoppler, T. Gutberlet, J. Voigt, F. Treubel, H.-U. Habermeier, G. Cristiani, B. Keimer, and C. Bernhard, Phys. Rev. B **71**, 140509(R) (2005).
[14] J. Chakhalian, J. W. Freeland, G. Srajer, J. Strempfer, G. Khaliullin, J. C. Cezar, T. Charlton, R. Dalgliesh, C. Bernhard, G. Cristiani, H.-U. Habermeier, and B. Keimer, Nat. Phys. **2**, 244 (2006).
[15] J. Hoppler, J. Stahn, Ch. Niedermayer, V. K. Malik, H. Bouyanfif, A. J. Drew, M. Rössle, A. Buzdin, G. Cristiani, H.-U. Habermeier, B. Keimer, and C. Bernhard, Nature Mater. **8**, 315 (2009).
[16] J. Hoppler, J. Stahn, H. Bouyanfif, V. K. Malik, B. D. Patterson, P. R. Willmott, G. Cristiani, H.-U. Habermeier, and C. Bernhard, Phys. Rev. B **78**, 134111 (2008).
[17] V. K. Vlasko-Vlasov, Y. K. Lin, D. J. Miller, U. Welp, G. W. Crabtree, and V. I. Nikitenko, Phys. Rev. Lett. **84**, 2239 (2000).
[18] L. Daillant and A. Gibaud, *X-Ray and Neutron Reflectivity: Principles and Applications*, Lecture Notes in Physics Monographs Vol. 58 (Springer, New York, 1999).
[19] F. Ott, C. R. Phys. **8**, 763 (2007).
[20] H.-U. Habermeier, G. Cristiani, R. K. Kremer, O. Lebedev, and G. van Tendeloo, Physica C **364-365**, 298 (2001).
[21] H. Fritzsche, Rev. Sci. Instrum. **76**, 115104 (2005).
[22] F. S. Bergeret, A. F. Volkov, and K. B. Efetov, Rev. Mod. Phys. **77**, 1321 (2005).
[23] L. G. Parratt, Phys. Rev. **95**, 359 (1954).
[24] H. Zabel, K. Theis-Bröhl, and B. P. Toperverg, in *Handbook of Magnetism and Advanced Magnetic Materials* (Wiley, New York, 2007), Vol. 3.
[25] F. Radu, V. Leiner, M. Wolff, V. K. Ignatovich, and H. Zabel, Phys. Rev. B **71**, 214423 (2005).
[26] E. Dagotto, T. Hotta, and A. Moreo, Phys. Rep. **344**, 1 (2001).
[27] C. Şen, G. Alvarez, and E. Dagotto, Phys. Rev. Lett. **98**, 127202 (2007).
[28] Unpublished.
[29] N. M. Nemes, M. García-Hernández, S. G. E. te Velthuis, A. Hoffmann, C. Visani, J. Garcia-Barriocanal, V. Peña, D. Arias, Z. Sefrioui, C. León, and J. Santamaría, Phys. Rev. B **78**, 094515 (2008).